*J. Fluid Mech.* (2000), *vol.* 408, *pp.* 39–52. Printed in the United Kingdom



# The effects of unstable stratification and mean shear on the chemical reaction in grid turbulence

By KOUJI NAGATA AND SATORU KOMORI

Department of Mechanical Engineering, Kyoto University,
Kyoto 606-8501, Japan

(Received 21 May 1998 and in revised form 16 November 1999)

The effects of unstable thermal stratification and mean shear on chemical reaction and turbulent mixing were experimentally investigated in reacting and non-reacting liquid mixing-layer flows downstream of a turbulence-generating grid. Experiments were carried out under three conditions: unsheared neutrally stratified, unsheared unstably stratified and sheared neutrally stratified. Instantaneous velocity and concentration were simultaneously measured using the combination of a laser-Doppler velocimeter and a laser-induced fluorescence technique. The results show that the turbulent mixing is enhanced at both large and small scales by buoyancy under unstably stratified conditions and therefore the chemical reaction is strongly promoted. The mean shear acts to enhance the turbulent mixing mainly at large scales. However, the chemical reaction rate in the sheared flow is not as large as in the unstably stratified case with the same turbulence level, since the mixing at small scales in the sheared neutrally stratified flow is weaker than that in the unsheared unstably stratified flow. The unstable stratification is regarded as a better tool to attain unsheared mixing since the shearing stress acting on the fluid is much weaker in the unstably stratified flow than in the sheared flow.

## 1. Introduction

Turbulent reactive flows can be seen in the atmospheric boundary layer with photochemical reactions, in turbulence with combustion and in many industrial reactors. It is, therefore, of great importance to elucidate the turbulent reactive–diffusive mechanism both in predicting the turbulent diffusion of reactive contaminants such as $NO_X$ and $SO_X$ exhausted from automobiles or power plants into the environment and in designing industrial combustors or reactors.

When two non-premixed reactants, A and B, are introduced into a turbulent flow, the chemical reactants are convected and mixed mainly by turbulent motions. The reaction rapidly proceeds by molecular diffusion at the complicatedly deformed interface between two reactive fluids. Therefore, the turbulence structure plays an important role in the progress of the chemical reaction until two reactants are perfectly mixed up to the minimum scale of turbulence.

One of the factors that modify the turbulence structure is the mean fluid shear. It is well known that the mean shear acts to enhance the turbulent mixing and hence the chemical reaction is promoted (e.g. Breidenthal 1981; Komori *et al.* 1991*a*). Besides the fluid shear, the turbulent mixing is enhanced by buoyancy under unstably stratified conditions (e.g. Pruitt, Morgan & Lourence 1973; Arya 1975; Komori *et al.* 1982),

and the chemical reaction is also expected to be promoted by buoyancy. Although extensive experimental and numerical studies on turbulent reacting flows have been performed over the past couple of decades, they were focused on either isothermal flows with no buoyancy effects or combustive flows in which the chemical reaction itself generates the buoyancy force. Thus, the buoyancy effects on the chemical reaction in stratified conditions are not well understood.

On the other hand, from the practical point of view, an unsheared mixing technology is required to avoid the destruction of the biocell or polymer molecules in bioreactors and polymerization reactors. Such unsheared mixing is expected to be achieved by means of buoyancy convection under unstably stratified conditions. However, it remains an interesting question which out of weak shear and buoyancy is more effective in promoting chemical reaction and mixing under weakly sheared or unsheared conditions.

The purpose of this study is, therefore, to experimentally investigate the effects of both unstable stratification and mean shear on chemical reaction and turbulent mixing. Simultaneous measurements of instantaneous velocity and concentration were conducted using a specially developed combination of laser-Doppler and laser-induced fluorescence techniques in reacting and non-reacting mixing-layer water flows downstream of a turbulence-generating grid in sheared or unstably stratified conditions.

## 2. Experiments

Figure 1(*a*) shows the measuring system and test apparatus. The test apparatus used was a water tunnel made of polymethylemethacrylate (PMMA), 1 m in length and $0.1 \times 0.1$ m in cross-section. A turbulence-generating grid was installed at the entrance to the test section, and it was of round-rod, square-mesh, single-biplain construction. The mesh size $M$ and the diameter of the rod $d$ were 0.02 and 0.003 m, respectively. The solidity of the grid was 0.28, which was slightly smaller than the value of 0.30 in Schedvin, Stegen & Gibson (1974), 0.31 in LaRue & Libby (1981), Stillinger, Helland & Van Atta (1983), and 0.34 in Comte-Bellot & Corrsin (1971). Aqueous solutions of the species A and B were separately pumped up from two big storage tanks to the head tanks, and then passed through the contraction, which was separated into upper and lower sections by a splitter plate. Table 1 shows the combinations of species A and B. For a non-reacting flow, species A was an aqueous solution with sodium fluorescein dye ($C_{20}H_{10}Na_2O_5$) and species B was fresh water without any chemical species (figure 1*b*). The concentration of the sodium fluorescein dye (species A) was $5 \times 10^{-5}$ mol m$^{-3}$. For the reacting flow, an irreversible second-order rapid reaction between acetic acid ($CH_3COOH$; species A) and ammonium hydroxide ($NH_4OH$; species B):

$$CH_3COOH + NH_4OH \rightarrow CH_3COONH_4 + H_2O, \tag{2.1}$$

was used (figure 1*b*). The initial concentrations of the two reacting species, $C_{A0}$ and $C_{B0}$, were set to the same value of 0.01 N. The sodium fluorescein dye was homogeneously premixed into both the solutions A and B at the same concentration of $5.0 \times 10^{-5}$ mol m$^{-3}$. For concentration measurements, the dependence of fluorescence intensity on the pH of the solution was used (Komori, Kanzaki & Murakami 1991*b*; Komori *et al.* 1993). The reaction rate constant, $k$, was of the order $10^8$ m$^3$ mol$^{-1}$ s$^{-1}$. The Damköhler number $\mathscr{D}a_L$ ($= \tau_1/\tau_3$), which is the ratio of the timescale of the turbulent diffusion $\tau_1$ ($= L/(\overline{q^2})^{1/2}$) to that of the chemical reaction $\tau_3$ ($= (k(C_{A0}C_{B0})^{1/2})^{-1}$) (Bennani, Gence & Mathieu 1985; Komori *et al.* 1991*b*), was nearly equal to $4 \times 10^5$,

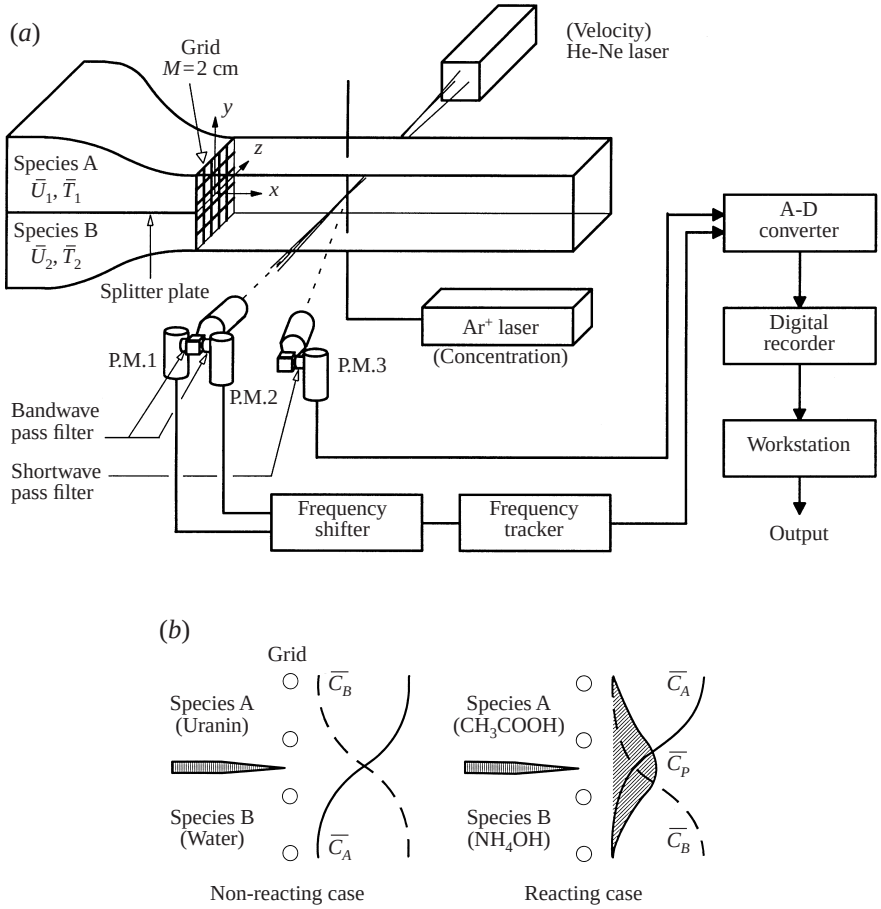


FIGURE 1. (*a*) Measuring system and test apparatus. (*b*) Flow conditions.

| | Species A | Species B | Reaction rate constant [$m^3\,mol^{-1}\,s^{-1}$] |
|---|---|---|---|
| Non-reacting case | $H_2O$ + uranin | $H_2O$ | 0 |
| Reacting case | $CH_3COOH$ + uranin | $NH_4OH$ + uranin | $10^8$ |

TABLE 1. Combinations of species A and B.

and the Damköhler number $\mathscr{D}a_\lambda\,(=\tau_2/\tau_3)$, which is the ratio of the timescale of the molecular diffusion $\tau_2\,(=\lambda^2/\mathscr{D})$ to that of the chemical reaction $\tau_3$ (Bennani *et al.* 1985), was nearly equal to $4\times10^9$. Here $L$ is the integral lengthscale, $\overline{q^2}$ is the turbulence kinetic energy, $\lambda$ is the microscale and $\mathscr{D}$ is the molecular diffusivity of mass. The values of $L$ and $\lambda$ estimated from the decay of $\overline{q^2}$ were 2.8 mm and 2.4 mm at $x/M = 6$, respectively.

| Run | $\Delta\overline{T}$ [K] | $\Delta\overline{U}$ [m s$^{-1}$] | $\overline{U}_{ave}$ [m s$^{-1}$] | $Re_M$ [–] | With or without reaction |
|---|---|---|---|---|---|
| I–NR | 0.0 | 0.0 | 0.125 | 2500 | no reaction |
| I–R | 0.0 | 0.0 | 0.125 | 2500 | reaction |
| II–NR | 10.0 | 0.0 | 0.125 | 2500 | no reaction |
| II–R | 10.0 | 0.0 | 0.125 | 2500 | reaction |
| III–NR | 0.0 | 0.03 | 0.125 | 2500 | no reaction |
| III–R | 0.0 | 0.03 | 0.125 | 2500 | reaction |
| IV–NR | 0.0 | 0.04 | 0.125 | 2500 | no reaction |
| IV–R | 0.0 | 0.04 | 0.125 | 2500 | reaction |

TABLE 2. Experimental conditions.

The experimental conditions are listed in table 2. The experiments were carried out in three types of flows. The first is the unsheared neutrally stratified flow with grid turbulence (hereinafter referred to as the *unsheared flow*) (Run I). For this flow, isothermal water was provided in both the upper and lower streams, and the mean velocities of the upper and lower streams, $\overline{U_1}$ and $\overline{U_2}$, were set to the same value of 0.125 m s$^{-1}$, so that a shear-free mixing layer was developed in the test section downstream of the turbulence-generating grid. The Reynolds number based on the mesh size $M$ and cross-sectionally averaged velocity $\overline{U}_{ave}$, $Re_M$, was 2500, and the turbulence Reynolds number based on the microscale, $Re_t$, was estimated to be 20 at $x/M = 6$.

The second type of flow is the unsheared unstable thermally stratified flow with grid turbulence (hereinafter referred to as the *unstably stratified flow*) (Run II). To generate the unstably stratified condition, cold and hot water were provided in the upper and lower streams, respectively. Thus, unstably stratified flow with an initial step temperature profile was generated behind the grid. The high-temperature water in the lower stream was heated by a boiler and the temperature was regulated in the storage tank by an electric heater connected to a thermometer. The initial temperature difference between the upper and lower streams, $\Delta\overline{T}\,(=\overline{T_2}-\overline{T_1})$, was set to 10 K. The mean velocities of the upper and lower streams, $\overline{U_1}$ and $\overline{U_2}$, were set to the same value of 0.125 m s$^{-1}$. The bulk Richardson number based on the initial temperature difference and cross-sectionally averaged velocity, $Ri_b\,(=-\beta g\Delta\overline{T}M/\overline{U}_{ave}^2)$, was $-2.60\times10^{-2}$, and the Grashof number, $Gr\,(=\beta g\Delta\overline{T}M^3/\nu^2)$, was $1.62\times10^5$, where $\beta$ is the thermal volumetric expansion coefficient, $g$ is the gravitational acceleration and $\nu$ is the kinematic viscosity.

The third type of flow is the sheared neutrally stratified flow with grid turbulence (hereinafter referred to as the *sheared flow*) (Runs III and IV). Isothermal water was provided in both the upper and lower streams, and the initial velocity difference between the upper and lower streams, $\Delta\overline{U}\,(=\overline{U_1}-\overline{U_2})$, was set to 0.03 m s$^{-1}$ (Run III) or 0.04 m s$^{-1}$ (Run IV) by fixing the cross-sectionally averaged velocity to the same value of 0.125 m s$^{-1}$ as in the unsheared flows. Therefore, the Reynolds number based on the mesh size, $Re_M$, was the same for all unsheared and sheared flows. The Reynolds numbers based on the initial velocity difference, $\Delta\overline{U}$, and the vorticity thickness of the mixing layer, $\delta_m\,(=\Delta\overline{U}/(\partial\overline{U}/\partial y)_{max})$, were estimated to be $8.0\times10^2$ and $1.1\times10^3$ at $x/M = 14$ for Runs III and IV, respectively. These values were close to the previous experiments (e.g. Breidenthal 1981).

Instantaneous velocity and concentration of species A were simultaneously mea-

sured using a combined measuring technique as shown in figure 1(*a*). The measuring technique combined a two-component laser-Doppler velocimeter (LDV) with a laser-induced fluorescence (LIF) method. The laser-Doppler velocimeter used here was a DANTEC 55X Modular system with a polarization beam splitter (55X24), a 40 MHz Bragg cell and a beam expander, and the laser was a 5 mW He-Ne laser with a 632.8 nm wavelength (Spectra Physics Model 106-1). The LDV unit for the velocity measurements was operated in the forward scattering mode. For the concentration measurements, a laser-induced fluorescence technique was used. The sodium fluorescein dye diffusing in the flow was illuminated by a high-power single-line mode argon-ion ($Ar^+$) laser of 0.8 W power and a 488 nm wavelength (LEXEL model 95-4). The He-Ne laser beams for the velocity measurements were shone from the sidewall of the test section, and a single beam of an $Ar^+$ laser for the concentration measurements was shone from the bottom wall. Both beams were focused by convex lenses and they intersected perpendicularly at a measuring point. The fluorescence from the measuring point was collected using an optical system (DANTEC 55X34). The focused and magnified fluorescence passed through a pinhole of 0.1 mm diameter, and it was received by a photomultiplier (HAMAMATSU R-777). The Doppler signals for the velocity measurements were collected by another optical system (DANTEC 55X34) connected to the photomultipliers (DANTEC 55X08). The wavelength difference between the Doppler signals from the scattered particles and the fluorescence from the sodium fluorescein dye was about 100 nm and therefore the two lights could be separated by installing optical filters between the optical system and the photomultipliers. Shortwave and bandwave pass filters were installed in front of the photomultipliers for the concentration and velocity measurements, respectively. The details of the spectra of fluorescence and scattered light and transmittance of optical filters are described in Komori *et al.* (1993). The spatial resolutions of velocity and concentration measurements were 1.0 mm and 100 μm, respectively. They were smaller than the dissipation scales of velocity and concentration fluctuations estimated from their dissipation spectra, which were 2.4 mm and 1.2 mm at $x/M = 6$, respectively. The measurements were made in the region of $6 \leqslant x/M \leqslant 20$. The sampling interval and the sample size were $2.5 \times 10^{-4}$ s and $2.4 \times 10^5$, respectively, and they gave reliable turbulence statistics. Statistical processing of the digitized data was done using a computer (SUN SPARC station).

## 3. Results and discussion

### 3.1. *Turbulence quantities*

Figure 2 shows the streamwise and vertical distributions of the turbulence intensities of the longitudinal and vertical velocity fluctuations. Here the velocity fluctuations are normalized by the square of the mean velocity, $\overline{U}^2$. In the unsheared flow (Run I), both the longitudinal and vertical velocity fluctuations have almost the same values and their decay follows a power law with the exponent of 1.58. The value of the exponent compares well with those obtained in the previous grid-generated water flow experiments (Nakamura, Sakai & Miyata 1987; Huq & Britter 1995). The correlation coefficient between $u$ and $v$, $R_{uv}$ $(= \overline{uv}/\sqrt{\overline{u^2}}/\sqrt{\overline{v^2}})$, was almost equal to zero in the whole region. The results show that an ideal grid-generated turbulence is developed in the present unsheared flow downstream of the turbulence grid. In the unstably stratified flow (Run II in figures 2*a* and 2*c*), the vertical velocity fluctuation is enhanced by buoyancy. Considering the buoyancy production term in the transport

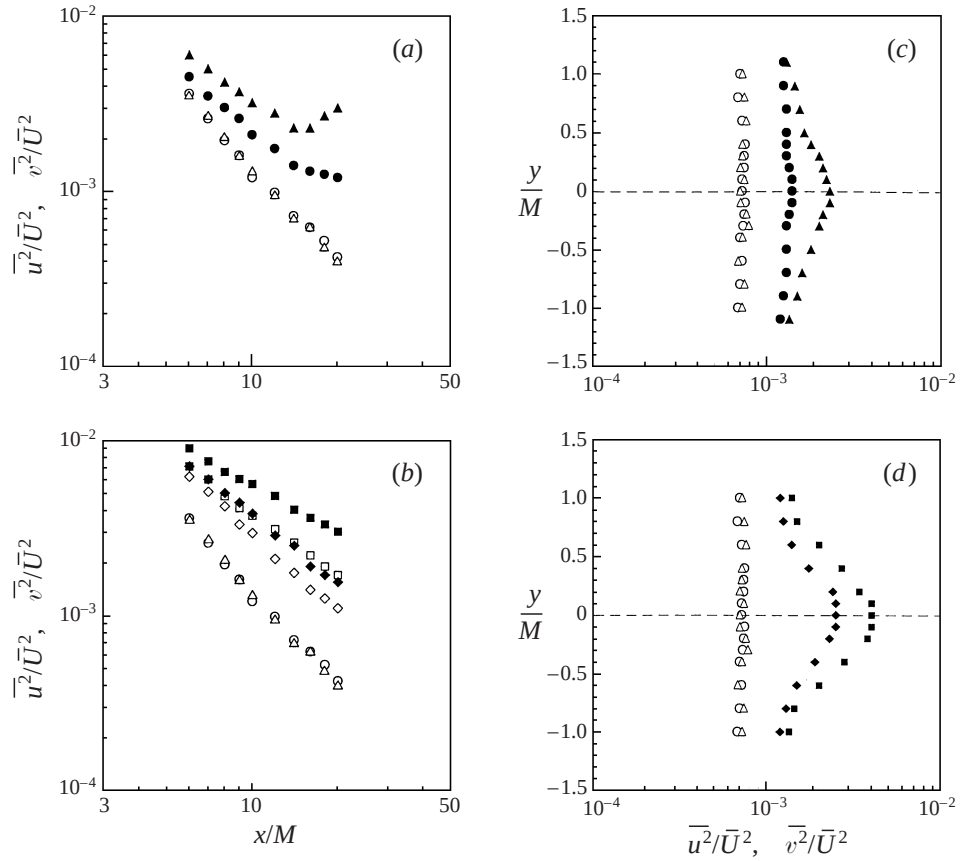


FIGURE 2. (*a*) Streamwise distributions of the turbulence intensities in unstably stratified flow: ○, $\overline{u^2}/\overline{U}^2$ in the unsheared flow (Run I); △, $\overline{v^2}/\overline{U}^2$ in the unsheared flow (Run I); ●, $\overline{u^2}/\overline{U}^2$ in the unstably stratified flow (Run II); ▲, $\overline{v^2}/\overline{U}^2$ in the unstably stratified flow (Run II). (*b*) Streamwise distributions of the turbulence intensities in sheared flow: ○, $\overline{u^2}/\overline{U}^2$ in the unsheared flow (Run I); △, $\overline{v^2}/\overline{U}^2$ in the unsheared flow (Run I); □, $\overline{u^2}/\overline{U}^2$ in the sheared flow with $\Delta\overline{U} = 0.03\,\mathrm{m\,s^{-1}}$ (Run III); ◇, $\overline{v^2}/\overline{U}^2$ in the sheared flow with $\Delta\overline{U} = 0.03\,\mathrm{m\,s^{-1}}$ (Run III). ■, $\overline{u^2}/\overline{U}^2$ in the sheared flow with $\Delta\overline{U} = 0.04\,\mathrm{m\,s^{-1}}$ (Run IV); ◆, $\overline{v^2}/\overline{U}^2$ in the sheared flow with $\Delta\overline{U} = 0.04\,\mathrm{m\,s^{-1}}$ (Run IV); (*c*) Vertical distributions of the turbulence intensities in the unstably stratified flow (Run II). Symbols as in (*a*). (*d*) Vertical distributions of the turbulence intensities in the sheared flow with $\Delta\overline{U} = 0.04\,\mathrm{m\ s^{-1}}$ (Run IV). Symbols as in (*b*).

equation of the vertical velocity fluctuation, $\overline{v^2}$:

$$\frac{\mathrm{D}\overline{v^2}}{\mathrm{D}t} = \underbrace{2\beta g\overline{v\theta}}_{\substack{\text{buoyancy}\\ \text{production}}} + 2\overline{\frac{p}{\rho}\frac{\partial v}{\partial y}} - 2\nu\overline{\frac{\partial v}{\partial x_k}\frac{\partial v}{\partial x_k}} - \frac{\partial}{\partial x_k}\left[\overline{v^2u_k} - \nu\frac{\partial\overline{v^2}}{\partial x_k} + 2\delta_{2k}\frac{\overline{vp}}{\rho}\right], \qquad (3.1)$$

we can interpret the increase of $\overline{v^2}$ by buoyancy. The longitudinal velocity fluctuation is also enhanced since the energy is redistributed from the vertical velocity fluctuation to the streamwise velocity fluctuation through the pressure–strain correlation term. (Note that the pressure–strain term acts to reduce the anisotropy of the flow.) In the sheared flows (Runs III and IV in figures 2*b* and 2*d*), the longitudinal velocity

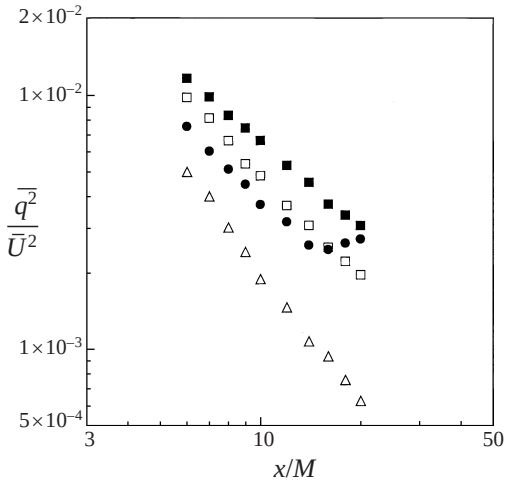


FIGURE 3. Streamwise distributions of the turbulence kinetic energy: △, unsheared flow (Run I); ●, unstably stratified flow (Run II); □, sheared flow with $\Delta\overline{U} = 0.03\,\mathrm{m\,s^{-1}}$ (Run III); ■, sheared flow with $\Delta\overline{U} = 0.04\,\mathrm{m\,s^{-1}}$ (Run IV).

fluctuation is enhanced by the mean shear. This behaviour can be explained by considering the shear production term in the transport equation of the longitudinal velocity fluctuation, $\overline{u^2}$:

$$\frac{\mathrm{D}\overline{u^2}}{\mathrm{D}t} = \underbrace{-2\overline{uv}\frac{\partial\overline{U}}{\partial y}}_{\textit{shear production}} + 2\overline{\frac{p}{\rho}\frac{\partial u}{\partial x}} - 2\nu\overline{\frac{\partial u}{\partial x_k}\frac{\partial u}{\partial x_k}} - \frac{\partial}{\partial x_k}\left[\overline{u^2u_k} - \nu\frac{\partial\overline{u^2}}{\partial x_k} + 2\delta_{1k}\frac{\overline{up}}{\rho}\right]. \qquad (3.2)$$

The vertical velocity fluctuation is also enhanced in consequence of the energy redistribution from the streamwise to the vertical velocity fluctuation. The comparison between $\overline{v^2}$ for the sheared flow with $\Delta\overline{U} = 0.04\,\mathrm{m\,s^{-1}}$ in figure 2(*b*) (Run IV, ◆) and that for the unstably stratified flow in figure 2(*a*) (Run II, ▲) shows that two distributions are almost equivalent around $x/M$=12–14. The vertical distributions of $\overline{u^2}$ and $\overline{v^2}$ in figures 2(*c*) and 2(*d*) show that the turbulence intensities around the centreline are larger than those near the edges. This means that the turbulence is mainly produced by buoyancy under unstably stratified condition and by shear under sheared condition. Figure 3 shows the distributions of the turbulence kinetic energy, $\overline{q^2}\,(=\overline{u_iu_i}/2)$. Here the spanwise velocity fluctuations, $\overline{w^2}$, were replaced by $\overline{u^2}$ for the unstably stratified flow (Komori *et al.* 1982) and by $\overline{v^2}$ for the sheared flows (Rogers & Moin 1987). The turbulence kinetic energy in the sheared flow with $\Delta\overline{U} = 0.03\,\mathrm{m\,s^{-1}}$ (Run III) is larger than that in the unstably stratified flow (Run II) in the region $x/M \leqslant 14$, and they become almost the same around $x/M$=14–16. For the sheared flow with $\Delta\overline{U} = 0.04\,\mathrm{m\,s^{-1}}$ (Run IV), $\overline{q^2}$ is larger than that for the unstably stratified flow in the region $x/M \leqslant 20$.

Figure 4 shows the streamwise distributions of the vertical mass fluxes of non-reactive and reactive species, normalized by the product of the mean velocity $\overline{U}$ and initial concentration of the species A, $C_{A0}$. In the unsheared flow (Run I), the vertical mass fluxes both in non-reacting and reacting flows decay in the streamwise direction. However, the difference in the vertical mass flux between the reacting and non-reacting flows is very small. The reason lies in the fact that the large-scale motions mainly

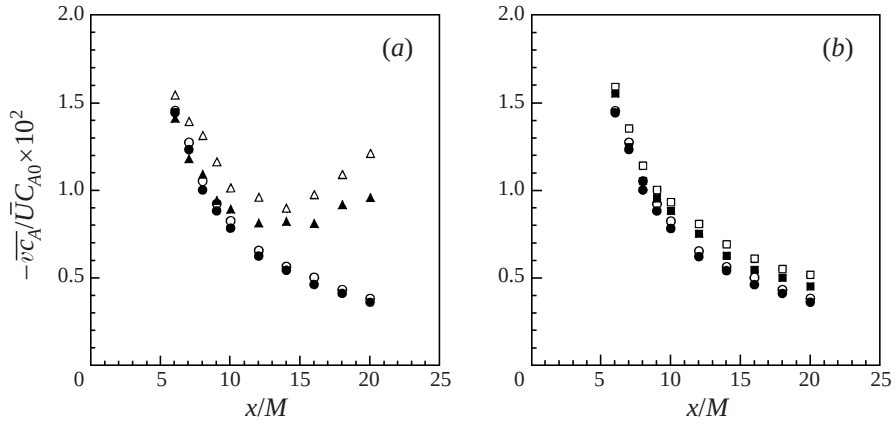


FIGURE 4. Streamwise distributions of the normalized vertical mass fluxes in (*a*) unstably stratified and (*b*) sheared flows: ○, unsheared flow without reaction (Run I-NR); ●, unsheared flow with reaction (Run I-R); △, unstably stratified flow without reaction (Run II-NR); ▲, unstably stratified flow with reaction (Run II-R); □, sheared flow without reaction (Run III-NR); ■, sheared flow with reaction (Run III-R).

contribute to the turbulent mass transfer, whereas the chemical reaction mainly occurs at smaller scales as inferred from both the power spectra of concentration fluctuation $c$ and the cospectra of $v$ and $c$ in figure 5(*a*). In the unstably stratified flow (Run II), the vertical mass flux is strongly enhanced by buoyancy, and the mass flux in the reacting flow becomes smaller than that in the non-reacting flow. This means that the fast progress of the chemical reaction results in the decrease of the mass flux of the reacting species, since the reacting species is converted by the reaction to the chemical product irrespective of the mass flux $\overline{vc_A}$. It can be seen from figure 5(*b*) that the effects of the chemical reaction spread to larger scales compared to the unsheared case. In the sheared flow (Run III), the vertical mass flux is enhanced by the shear. However, the difference in the mass flux between non-reacting and reacting cases is very small as in the unsheared case. This can also be seen in the power spectra and cospectra in figure 5(*c*).

### 3.2. *Mean concentration profiles*

Figures 6 and 7 show the streamwise and vertical distributions of the mean concentrations of chemical species A and chemical product P. The vertical concentration profiles in figure 7 were obtained at $x/M = 14$. Here the mean concentrations are normalized by the initial concentration of species A, $C_{A0}$. The mean concentrations of the product P were estimated by

$$\overline{C_P}/C_{A0} = 2(\overline{C_A^*} - \overline{C_A})/C_{A0}. \tag{3.3}$$

Here the asterisk denotes the concentration of species A in the non-reacting flow. Note that $\overline{C_P}$ is the sum of the product locally generated and that transported from upstream. The streamwise distributions in figure 6 show that the fast progress of the chemical reaction results in more rapid decrease of species A and more rapid increase of the product P in the streamwise direction in the unstably stratified flow than in the sheared flow. Furthermore, the vertical distributions in figures 7(*b*) and 7(*c*) clearly show that the chemical reaction is promoted more in the unstably stratified flow than in the sheared flow. To quantitatively compare the effects of the unstable stratification

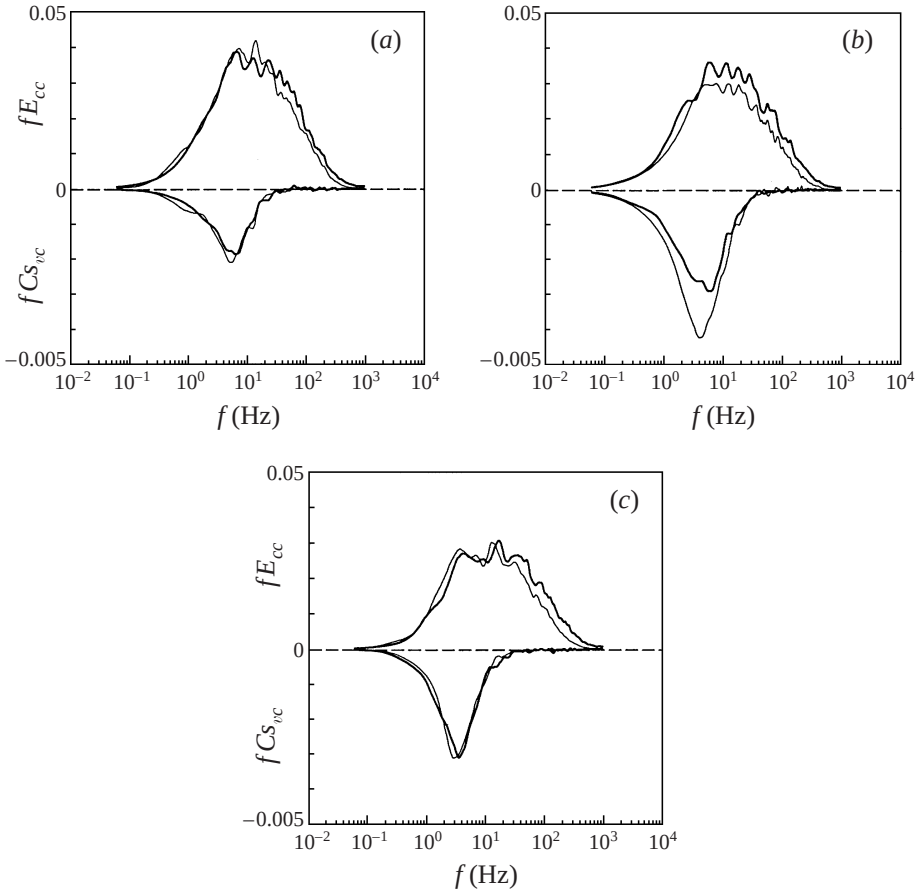


FIGURE 5. Power spectra of concentration $c$ and cospectra of $v$ and $c$ in the ($a$) unsheared ($b$) unstably stratified and ($c$) sheared flows: ——, without reaction; ——, with reaction. The power spectra and cospectra are normalized by $\overline{c^2}$ and $\overline{U}C_{A0}$, respectively.

and mean shear on the chemical reaction, the mean concentration of the product P was integrated along the vertical $y$-axis at $x/M = 14$ (Breidenthal 1981):

$$P_T = \int_{-\infty}^{\infty} \frac{\overline{C_P}(y)}{C_{A0}} \mathrm{d}y. \tag{3.4}$$

The amount of the chemical product, $P_T$, is compared in figure 8 between the unstably stratified flow and the sheared flow. The total amount of the reaction product in the unstably stratified flow (Run II) becomes 1.83 times larger than that in the unsheared flow (Run I), whereas $P_T$ in the sheared flow with the same level of turbulence kinetic energy as in the unstably stratified flow (Run III) is only 1.18 times larger than that in the unsheared flow (Run I). However, the vertical concentration gradients of species A in the non-reacting flows are not strictly the same for the unstably stratified (Run II) and sheared (Run III) flows. The difference may suggest that the convection rates of the chemical species are different for the two flows. Figure 7($d$) shows the vertical profiles of the mean concentrations in the sheared flow with $\Delta\overline{U} = 0.04\,\mathrm{m\,s^{-1}}$. Although the vertical concentration gradients of species A in non-reacting conditions are almost the same for the unstably stratified flow and the sheared flow with

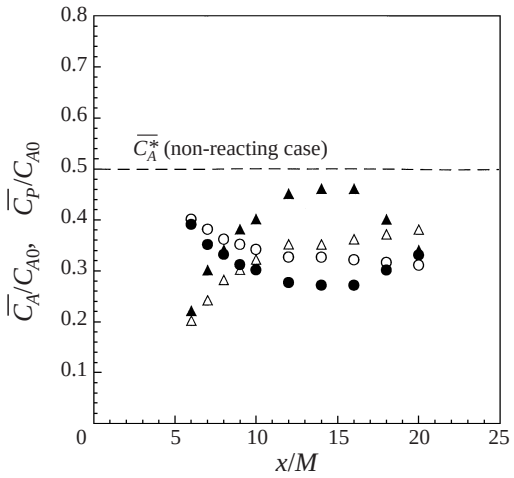


FIGURE 6. Streamwise distributions of the mean concentrations: ●, $\overline{C_A}$ in the unstably stratified flow (Run II-R); ▲, $\overline{C_P}$ in the unstably stratified flow (Run II-R); ○, $\overline{C_A}$ in the sheared flow (Run III-R); △, $\overline{C_P}$ in the sheared flow (Run III-R).

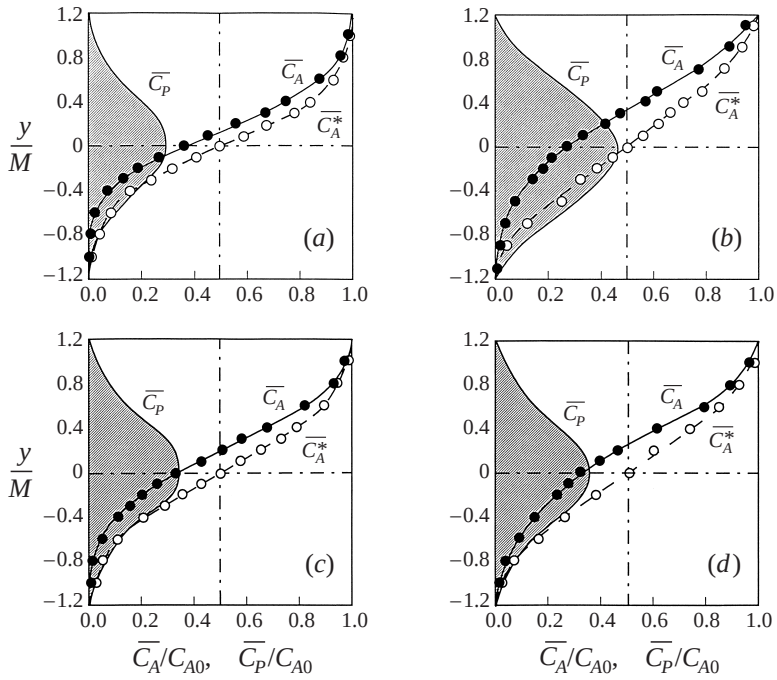


FIGURE 7. Vertical profiles of the mean concentrations of species A and product P in the (*a*) unsheared (Run I), (*b*) unstably stratified (Run II), (*c*) sheared ($\Delta\overline{U} = 0.03\,\mathrm{m\,s^{-1}}$, Run III) and (*d*) sheared ($\Delta\overline{U} = 0.04\,\mathrm{m\,s^{-1}}$, Run IV) flows: ○, without reaction; ●, with reaction.

$\Delta\overline{U} = 0.04\,\mathrm{m\,s^{-1}}$, the chemical reaction rate in the unstably stratified flow is larger than that in the sheared flow. In fact, $P_T$ estimated by (3.4) is only 1.24 times larger than that in the unsheared flow (figure 8). Furthermore, for the sheared flow with $\Delta\overline{U} = 0.04\,\mathrm{m\,s^{-1}}$, the intensity of the vertical velocity fluctuation was almost equivalent to the unstably stratified case (Run II) as shown in figure 2.

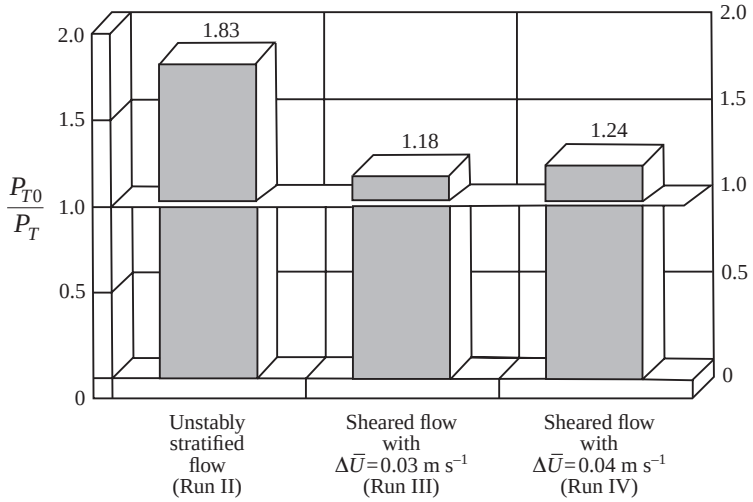


FIGURE 8. Comparison between the amounts of the chemical product in the unstably stratified and sheared flows.

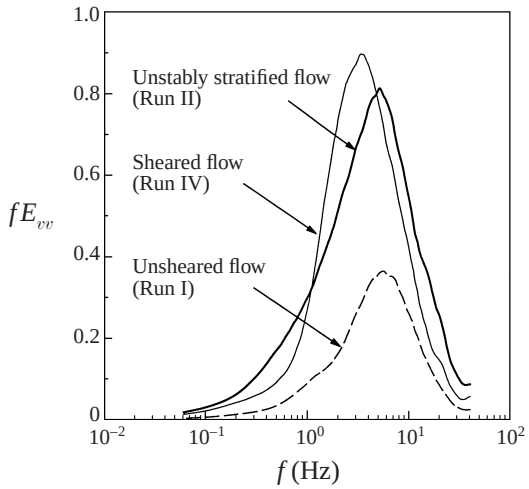


FIGURE 9. Power spectra of the vertical velocity fluctuations in the unsheared (- - - - -), unstably stratified (——) and sheared (——) flows.

### 3.3. *The effects of unstable stratification and mean shear on the chemical reaction and turbulent mixing*

Several results in the above subsection showed that the chemical reaction is promoted more in the unstably stratified flow than in the sheared flow even if the turbulence kinetic energy, the intensity of the vertical velocity fluctuation or the vertical concentration gradient of non-reacting species A has the same value for the two flows. This may be attributed to the difference in the turbulence structure between the two types of flows. To investigate the difference in the turbulence structure between the unstably stratified and sheared flows, the power spectrum of the vertical velocity fluctuation was computed at $x/M = 14$. The one-dimensional power spectrum of the vertical

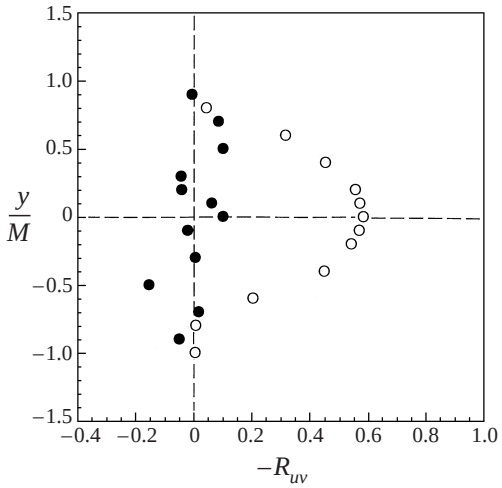


FIGURE 10. Vertical profiles of the Reynolds stress in the unstably stratified and sheared flows: ●, unstably stratified flow (Run II); ○, sheared flow with $\Delta\overline{U} = 0.03\,\mathrm{m\,s^{-1}}$ (Run III).

velocity fluctuation, $E_{vv}(f)$, is defined as

$$\int_0^\infty E_{vv}(f)\,\mathrm{d}f = \overline{v^2}. \tag{3.5}$$

Figure 9 shows the power spectra in the unsheared, unstably stratified and sheared flows. The area bounded by the power spectra multiplied by the frequency $f$ corresponds to the intensity of the vertical velocity fluctuation. For the unstably stratified case, the buoyancy acts to enhance the turbulent mixing at small scales as well as at large scales. This is attributed to the fact that the large Prandtl number ($Pr > 1$) induces a relative increase of the available potential energy at small scales, compared to the vertical turbulence kinetic energy (Komori & Nagata 1996; Hanazaki & Hunt 1996). On the other hand, the mean shear acts to enhance the turbulent mixing mainly at large scales (Komori & Nagata 1996; Deissler 1961). The small-scale eddies in a shear flow are generated by the interaction between large-scale eddies produced by shear (Hunt & Vassilicos 1991), but in the present low Reynolds number flow the small-scale motions are not as enhanced by shear. To promote the chemical reaction in a turbulent flow, the turbulent motion has to distort or stretch the interface occupied by the chemical product and to promote the turbulent and molecular mixing between two reacting species. In this sense, the small-scale eddies generated by buoyancy work to distort and stretch the interface between chemical species A and B under unstably stratified conditions and therefore the chemical reaction is strongly promoted. On the other hand, in the sheared flow, the mean shear acts to enhance the turbulent mixing mainly at large scales and hence the chemical reaction is not as promoted as in the unstably stratified case.

### 3.4. *Advantage of unstable stratification for developing an unsheared mixing technology*

Figure 10 shows the vertical profiles of the Reynolds stresses in the correlation coefficient form at $x/M = 14$ in the unstably stratified and sheared flows (Runs II and III). The Reynolds stress is almost equal to zero under unstably stratified conditions, whereas it becomes very large in the central region around $y/M = 0$ in the sheared flow. This means that the shearing stress acting on the fluid is much weaker

in the unstably stratified flow than in the sheared flow. The result, together with the amounts of the chemical product in figure 8, suggests that unstable stratification is a better technology for promoting the chemical reaction and turbulent mixing under unsheared conditions. The technology may be useful for bioreactors or polymerization reactors in which weakly-sheared mixing is required.

## 4. Conclusions

The effects of unstable stratification and mean shear on a rapid chemical reaction and turbulent mixing were experimentally investigated in both reacting and non-reacting water mixing-layer flows downstream of turbulence-generating grid. The main results from this study can be summarized as follows.

(i) Turbulent mixing is enhanced at both large and small scales by buoyancy under unstably stratified conditions, and the chemical reaction is strongly promoted by the buoyant convection.

(ii) The mean fluid shear acts to enhance the turbulent mixing mainly at large scales but the chemical reaction rate is not as large as in the unstably stratified case with the same turbulence level.

(iii) Unstable stratification is regarded as a better tool for promoting the chemical reaction and turbulent mixing under unsheared conditions since the shearing stress acting on the fluid is much weaker in the unstably stratified flow than in the sheared flow.

The authors would like to thank Messrs H. Matsumoto and H. Horibe for their help in conducting experiments. This work was supported by the Japanese Ministry of Education, Science and Culture through grants-in-aid (No. 11555059) and the KAWASAKI STEEL 21st Century Foundation.

## REFERENCES

Arya, S. P. S. 1975 Buoyancy effects in a horizontal flat-plate boundary layer. *J. Fluid Mech.* **68**, 321–343.

Bennani, A., Gence, J. N. & Mathieu, J. 1985 The influence of a grid-generated turbulence on the development of chemical reaction. *AIChE J.* **31**, 1157–1166.

Breidenthal, R. 1981 Structure in turbulent mixing layers and wakes using a chemical reaction. *J. Fluid Mech.* **109**, 1–24.

Comte-Bellot, G. & Corrsin, S. 1971 Simple Eulerian time correlation of full- and narrow-band velocity signals in grid-generated 'isotropic' turbulence. *J. Fluid Mech.* **48**, 273–337.

Deissler, R. G. 1961 Effects of inhomogeneity and of shear flow in weak turbulence fields. *Phys. Fluids* **4**, 1187–1198.

Hanazaki, H. & Hunt, J. C. R. 1996 Linear processes in unsteady stably stratified turbulence. *J. Fluid Mech* **249**, 415–440.

Hunt, J. C. R. & Vassilicos, J. C. 1991 Kolmogorov's contribution to the physical and geometrical understanding of small-scale turbulence and recent developments. *Proc. R. Soc. Lond.* A **434**, 183–210.

Huq, P. & Britter, R. E. 1995 Mixing due to grid-generated turbulence of a two-layer scalar profile. *J. Fluid Mech.* **285**, 17–40.

Komori, S., Hunt, J. C. R., Kanzaki, T. & Murakami, Y. 1991*a* The effects of turbulent mixing on the correlation between two species and on concentration fluctuation in non-premixed reacting flows. *J. Fluid Mech.* **228**, 629–659.

Komori, S., Kanzaki, T. & Murakami, Y. 1991*b* Simultaneous measurements of instantaneous concentrations of two reacting species in a turbulent flow with a rapid reaction. *Phys. Fluids* A **3**, 507–510.

Komori, S. & Nagata, K. 1996 Effects of molecular diffusivities on counter-gradient scalar and momentum transfer in strongly stable stratification. *J. Fluid Mech.* **324**, 205–237.

Komori, S., Nagata, K., Kanzaki, T. & Murakami, Y. 1993 Measurements of mass flux in a turbulent liquid flow with a chemical reaction. *AIChE J.* **39**, 1611–1620.

Komori, S., Ueda, H., Ogino, F. & Mizushina, T. 1982 Turbulence structure in unstably-stratified open-channel flow. *Phys. Fluids* **25**, 1539–1546.

LaRue, J. C. & Libby, P. A. 1981 Thermal mixing layer downstream of half-heated turbulence grid. *Phys. Fluids*, **24**, 597–603.

Nakamura, I., Sakai, Y. & Miyata, M. 1987 Diffusion of matter by a non-buoyant plume in grid-generated turbulence. *J. Fluid Mech.* **178**, 379–403.

Pruitt, W. O., Morgan, D. L. & Lourence, F. J. 1973 Momentum and mass transfers in the surface boundary layer. *Q. J. R. Met. Soc.* **99**, 370–386.

Rogers, M. M. & Moin, P. 1987 The structure of the vorticity field in homogeneous turbulent flows. *J. Fluid Mech.* **176**, 33–66.

Schedvin, J., Stegen, G. R. & Gibson, C. H. 1974 Universal similarity at high grid Reynolds numbers. *J. Fluid Mech.* **65**, 561–579.

Stillinger, D. C., Helland, K. N. & Van Atta, C. W. 1983 A closed-loop gravity-driven water channel for density-stratified shear flows. *J. Fluid Mech.* **131**, 73–89.